

EXPERIMENTAL IMPLEMENTATION OF MULTIPLE-INPUT MULTIPLE-OUTPUT ACTIVE VIBRATION CONTROL ON VIBRATION ISOLATION SYSTEMS

Peng Zhang, Fangpo He

Flinders University, School of Computer Science, Engineering and Mathematics, Adelaide, Australia email: michael.zhang@flinders.edu.au, fangpo.he@flinders.edu.au

This paper presents the design and implementation of a multi-input multi-output (MIMO), multiple-mode, active vibration-cancellation scheme for vibration isolation systems. A flexible rectangular plate that is subjected to an existing environmental disturbance introduced at the foundation of the plate, is used to mimic real-life scenarios of many mechanical structures. The control goal is to keep the plate vibration-free within a frequency range of concern, regardless of the continuous disturbance at the base. The plate is supported by three feet (loudspeakers), mimicking a non-ideal asymmetrical structure in a realistic situation. System identification techniques that incorporate multiple-degree-of-freedom polynomial curve fitting methods are used to produce a sound mathematical model of the plate that is verified through experiment. A centralized MIMO positive position feedback (PPF) control strategy that is capable of controlling multiple modes of the structure and avoiding potential control spillover problems, is then developed. The parameters of the controller is optimized using H_{∞} norm. The stability of the resulting closed-loop optimal PPF control system is presented. The existing three feet (loudspeakers) of the plate form three pairs of collocated sensors and actuators that further minimize potential spillover possibilities. The real-time controller is implemented on a dSPACE data acquisition and control board utilizing Matlab Simulink® and Real-Time Workshop® software. Both simulation and experiment studies are carried out systematically to verify each stage of the design and implementation. The real-time experimental results show that the compensated system can achieve up to 16.928 dB (or 85.757%) attenuation of the vibrations, which clearly demonstrate the effectiveness of the MIMO optimal PPF controller in suppressing the vibrations within the frequency range of concern. The proposed control scheme can be effectively applied to larger structures that are potentially vulnerable to environmental disturbances, and the resultant vibration isolation systems are sufficient in a wider range of frequencies.

Keywords: MIMO Multiple-Mode Active Vibration Control, Optimal PPF, Vibration Isolation Systems, Multivariable System Identification, Real-Time Control System Implementation

1. Introduction

A large flexible plate mounted on a vibrating base can be regarded as an ordinary representative model for a number of vibration isolation systems. A plate that is supported by three feet, forming a non-ideal asymmetrical structure which can mimic many realistic systems in real-life scenarios, is chosen for this study. This type of systems can be difficult to control due to the fact that they are

1

distributed-parameter systems and often contain a large amount of vibration modes with highly resonant behaviour near the structure's natural frequencies. In most cases, however, only a small number of dominant modes within a specified frequency range of concern is required to be controlled. Consequently, uncontrolled modes may lead to the problem of spill-over [1]. The spill-over effect is of major concern especially when sensors and actuators are poorly modelled and the amount of sensor/actuator pairs is limited [2]. One efficient way to avoid the spill-over effect is based on the technique of using collocated sensors and actuators [3]. To this end, several principle methods have been proposed in the literature that can add sufficient damping to the structure and guarantee the closed-loop stability of the system. Principle methods that can be used for controlling multiple-mode vibrations in flexible structures include positive position feedback (PPF) control [3], independent modal space control (IMSC) [4], and resonant control [5].

PPF control was first introduced by Goh and Caughey [3] using collocated sensor/actuator pairs. One advantage of PPF control lies in its insensitivity to spill-over effect as the controller uses a second-order compensator that rolls off quickly at high frequencies. MIMO PPF control has been successfully implemented in many applications, including: a beam structure with two inputs and two outputs [6], a sandwich plate structure with four sensors and two actuators [7], a grid structure [8], and even some non-collocated sensor/actuator systems [9].

IMSC was first proposed by Meirovich who used a modal filter to control each mode separately to avoid the spill-over effect [4]. Many modifications and improvements have been made to the original IMSC to optimize its performance in reducing spill-over [10]. One critical issue associated with IMSC is the fact that for each mode to be controlled, one pair of sensor/actuator is required [11]. Also, IMSC incurs a relatively high computational load, as it needs to calculate the highest energy mode continuously. These disadvantages limit the possibility of extending IMSC into larger systems.

Resonant control is based on the characteristics of a resonant system, and possesses many advantages over the other control methodologies [12] [13]. Firstly, the gain selection for each mode of the resonant controller is independent, which can reduce the computational load required. Secondly, it is possible for a resonant controller to use one pair of sensor/actuator to control multiple modes, thus reducing the complexity of the resulting control system. However, resonant control also has many shortcomings. The most critical shortcoming lies in its limitation in adding ample damping to the structure as compared to PPF and IMSC strategies [3]. Unlike resonant controllers, PPF controllers are able to provide a higher level of damping, while being able to control multiple modes using one pair of sensor/actuator.

Based on the above analysis, a centralized MIMO PPF control methodology is chosen to be designed and implemented to control the first three modes of the non-ideal asymmetric plate-structured vibration isolation system. A multiple-degree-of-freedom polynomial curve fitting technique is used to produce a valid model of the multivariable system. The stability condition of the resulting control system is derived, which guarantees the performance of the closed-loop system over the range of frequency of concern.

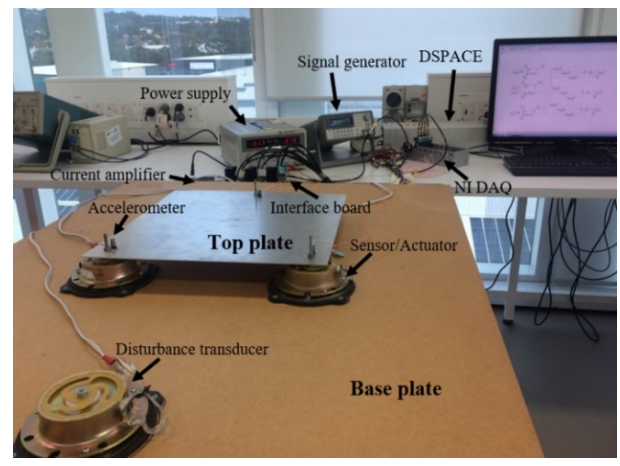
The rest of this paper is organized as follows. Section 2 discusses the system modelling process including the physical system setup, the system identification, and the model validation. In Section 3, the MIMO PPF controller is designed, the stability condition of the resulting control system is derived, and the performance of the closed-loop system is evaluated via simulation. The implementation of the control system and the experimental test on the physical system are performed in Section 4, which verifies the expected control effect. Meaningful conclusions are drawn in Section 5.

2. System Modelling

2.1 Physical System

The physical vibration isolation system is constructed using two (top and base) plates as shown in

Fig. 1. The base plate is vibrated constantly by signal w introduced from a disturbance transducer that is driven by a signal generator. The $400 \text{mm} \times 400 \text{mm} \times 1.5 \text{mm}$ top plate (density $\rho = 2.77 \times 10^{-12} \text{ m/V}$ and Yong's Modulus $E = 7.00 \times 10^{10} \text{ M/m}^2$) is bonded with the base plate using three loudspeakers acting as sensors and actuators (namely, transducers T1, T2, and T3). The output signals from the transducers are sensed by the interface board who performs the communication between the plant and the dSPACE DS1103 digital controller. The control signals, once generated by the controller, are injected into the plant via the same route using the actuation function of the transducers. The control goal is to keep the top plate vibration free while letting it be constantly subjected to the disturbance introduced from the base plate. Fig. 2 shows the schematic of the experimental setup.



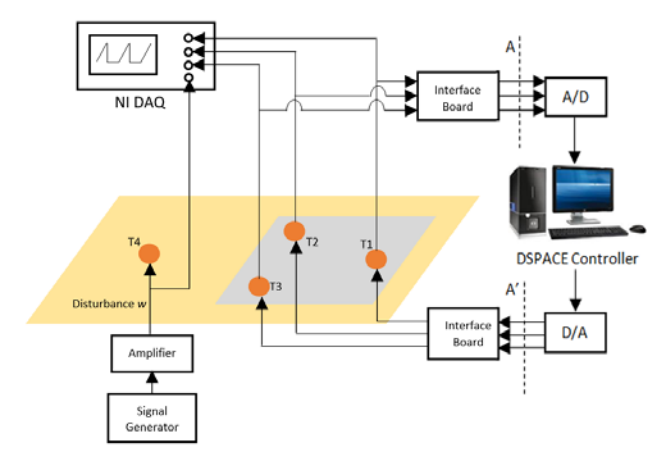


Fig. 1. Physical system

Fig. 2. Schematic of experimental setup

2.2 Multivariable System Identification

To generate a valid model of the physical system for the purpose of the controller design, an open-loop multivariable system identification study is carried out. For the open-loop modelling analysis, points A and A' in Fig. 2 are opened. An amplified sinusoidal signal whose frequency is swept between 20 Hz and 60 Hz is generated using a signal generator and is injected, respectively, into T1, T2, and T3 as input signals u_1 , u_2 , and u_3 to each of the transducers. For each input signal u_j (j = 1, 2, 3) acting alone, three output signals y_{1j} , y_{2j} , y_{3j} from T1, T2, and T3 are measured via accelerometers simultaneously, and the four signals are sent to the data acquisition system (NI DAQ) to generate the respective frequency response function (FRF) of the system:

$$H_{ij}(s) = \frac{Y_{ij}(s)}{U_i(s)} \qquad (i = 1, 2, 3)$$
 (1)

A 3×3 transfer matrix of the system, $\mathbf{H}(s)$, representing the model of the plant (including the top plate and the three sensor/actuator pairs) is thus formed as:

$$\mathbf{H}(\mathbf{s}) = \begin{bmatrix} H_{11} & H_{12} & H_{13} \\ H_{21} & H_{22} & H_{23} \\ H_{31} & H_{32} & H_{33} \end{bmatrix}$$
(2)

Fig. 3 shows the plate layout for the open-loop modelling analysis.

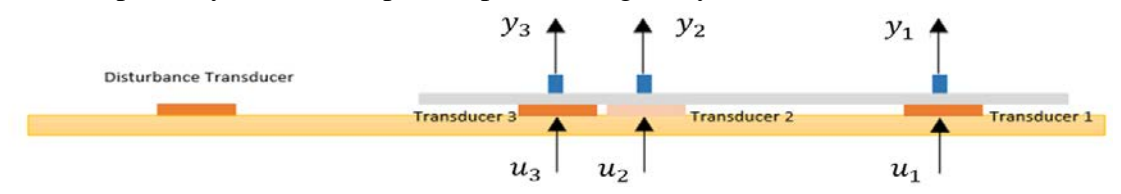


Fig. 3. Plate layout for modelling analysis

The measured 3×3 FRFs, $H_{ij}(s)$ (i, j = 1, 2, 3), for the open-loop system are plotted in Fig. 4 in black. To model the plant mathematically, a multiple-degree-of-freedom polynomial curve fitting

method is applied to each of the measured FRF curves to produce the corresponding transfer function, $H_{ii}(s)$, expressed as:

$$H_{ij}(s) = \sum_{k=1}^{N} \left(\frac{\varphi_{ij}^{k} \varphi_{ij}^{k'}}{s^{2} + 2\zeta_{ij}^{k} \omega_{ij}^{k} s + \omega_{ij}^{k^{2}}} \right) = \sum_{k=1}^{N} \left(\frac{r_{ij}^{k}}{s - \lambda_{ij}^{k}} + \frac{r_{ij}^{k^{*}}}{s - \lambda_{ij}^{k^{*}}} \right)$$
(3)

 $H_{ij}(s) = \sum_{k=1}^{N} \left(\frac{\varphi_{ij}^{k} \varphi_{ij}^{k'}}{s^{2} + 2\zeta_{ij}^{k} \omega_{ij}^{k} s + \omega_{ij}^{k^{2}}} \right) = \sum_{k=1}^{N} \left(\frac{r_{ij}^{k}}{s - \lambda_{ij}^{k}} + \frac{r_{ij}^{k^{*}}}{s - \lambda_{ij}^{k^{*}}} \right)$ with $\lambda_{ij}^{k} = -\zeta \omega_{ij}^{k} + j \omega_{ij}^{k} \sqrt{1 - \zeta_{ij}^{k^{2}}}$ and $\lambda_{ij}^{k^{*}} = -\zeta \omega_{ij}^{k} - j \omega_{ij}^{k} \sqrt{1 - \zeta_{ij}^{k^{2}}}$ where i, j, and k represent the i^{th} output component, the j^{th} input, and the k^{th} mode, respectively, and number N is large enough to enable (3) to represent the true model of the plant. While the damping ratios, ζ_{ij}^k , the natural frequencies, ω_{ij}^k , and the magnitudes, r_{ij}^k , in (3) can be obtained directly from the curve fitting technique, the mode shapes, φ_{ij}^k , in (3) need to be calculated via:

$$\varphi_{ij}^k = r_{ij}^k * 2\omega_{ij}^k \sqrt{1 - \zeta_{ij}^{k^2}} \tag{4}$$

For the chosen physical system, the frequency range of concern is within 20 to 40 Hz where three resonance frequencies for each of the measured FRFs are clearly shown in Fig. 4. A truncated model of the system is thus formed in which each of the 3×3 FRFs expressed in (3) is shortened to include its first three modes only. The resultant FRFs are expressed as:

$$\bar{H}_{ij}(s) = \sum_{k=1}^{3} \left(\frac{\varphi_{ij}^{k} \varphi_{ij}^{k'}}{s^{2} + 2\zeta_{ij}^{k} \omega_{ij}^{k} s + \omega_{ij}^{k^{2}}} \right)$$
 (5)

and are plotted in Fig. 4 in red. It can be seen from Fig. 4 that the truncated model relatively matches the true model especially when comparing the magnitudes of the dominant 2nd and 3rd modes. Therefore, $\overline{H}_{ii}(s)$ can be considered as a valid simplified model of the plant based on which the MIMO PPF controller of the system is to be designed.

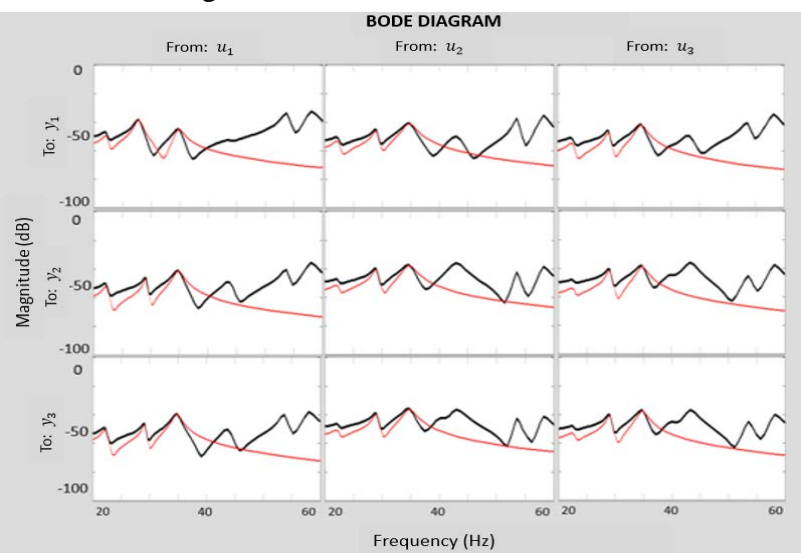


Fig. 4. Simulated truncated model FRFs (red) vs. measured true model FRFs (black)

3. Positive Position Feedback Control

3.1 **Controller Design**

In essence, a PPF controller receives the displacement response of a structure and provides the structure with a control input force that aims to damp out the structure's unwanted vibrations. Fig. 5 illustrates a MIMO PPF closed-loop system where the output signals Y(s) are sent to the PPF controller to produce the active damping forces $\mathbf{U}(s)$. The controller contains a set of parameter matrices, the values of which are to be designed.

To effectively control the three-input three-output plate system, simplifications in relation to the

system parameters contained in $\overline{H}_{ij}(s)$ (i, j = 1, 2, 3) in (5) need to be introduced. As the system is formed by a non-ideal asymmetrical structure, for a given k^{th} mode (k = 1, 2, 3), the damping ratios ζ_{ij}^k in the 3×3 $\overline{H}_{ij}(s)$ are all different (with the largest deviation of 0.01), and so do the natural frequencies ω_{ij}^k (with the largest deviation of 1.16 Hz). A common damping ratio, ζ_k (k = 1, 2, 3), is then chosen to be the maximum damping ratio identified among all ζ_{ij}^k for the k^{th} mode, and a common natural frequency, ω_k (k=1,2,3), is set to be the average value of all ω_{ij}^k for the k^{th} mode. The overall closed-loop system can then be written as [14]:

Structure:
$$\ddot{\xi} + D\dot{\xi} + \Omega\xi = C^T G \eta$$
 (6)

Compensator:
$$\ddot{\eta} + D_c \dot{\eta} + \Omega_c \eta = \Omega_c C \xi$$
 (7)

where ξ is the structure coordinate, η is the compensator coordinate, matrices D, Ω , and C contain the system parameters that are known in prior:

$$\mathbf{D} = \begin{bmatrix} 2\zeta_1 \omega_1 & & & \\ & 2\zeta_2 \omega_2 & & \\ & & 2\zeta_3 \omega_3 \end{bmatrix}, \ \mathbf{\Omega} = \begin{bmatrix} \omega_1^2 & & & \\ & \omega_2^2 & & \\ & & & \omega_3^2 \end{bmatrix}, \ \mathbf{C} = \begin{bmatrix} \varphi_{11} & \varphi_{12} & \varphi_{13} \\ \varphi_{21} & \varphi_{22} & \varphi_{23} \\ \varphi_{31} & \varphi_{32} & \varphi_{33} \end{bmatrix}$$

and matrices $\mathbf{D_c}$, $\mathbf{\Omega_c}$, and \mathbf{G} contain the damping ratios ζ_{ck} , natural frequencies ω_{ck} , and gains g_k (k

= 1, 2, 3) of the MIMO PPF controller, all of which are to be designed:
$$\mathbf{D_c} = \begin{bmatrix} 2\zeta_{c1}\omega_{c1} \\ 2\zeta_{c2}\omega_{c2} \\ 2\zeta_{c3}\omega_{c3} \end{bmatrix}, \quad \mathbf{\Omega_c} = \begin{bmatrix} \omega_{c1}^2 \\ \omega_{c2}^2 \\ \omega_{c3}^2 \end{bmatrix}, \quad \mathbf{G} = \begin{bmatrix} g_1 \\ g_2 \\ g_3 \end{bmatrix}$$

For the purpose of effective suppression of resonant behavior of the system at the modes of concern, ω_{ck} (k=1, 2, 3) are set to be the same as those of the structure (i.e., $\Omega_c = \Omega$) [15]. To provide sufficient damping to the structure, ζ_{ck} and g_k (k = 1, 2, 3) are designed separately using other means.

3.2 Close-loop stability analysis:

To prove the closed-loop stability of the MIMO PPF control system, define:

$$\mathbf{\eta} = \mathbf{G}^{-1/2} \mathbf{\Omega}_{\mathbf{c}}^{1/2} \mathbf{\Psi} \tag{8}$$

 $\eta = \mathbf{G}^{-1/2} \Omega_{\mathbf{c}}^{1/2} \Psi$ Substituting (8) into (6) and (7), and multiplying (7) with $\Omega_{\mathbf{c}}^{-T/2} \mathbf{G}^{T/2}$, we obtain: $\ddot{\xi} + \mathbf{D}\dot{\xi} + \Omega \xi = \mathbf{C}^T \mathbf{G}^{1/2} \Omega_{\mathbf{c}}^{1/2} \Psi$ $\ddot{\psi} + \mathbf{D}_{\mathbf{c}}\dot{\psi} + \Omega_{\mathbf{c}}\psi = \Omega_{\mathbf{c}}^{1/2} \mathbf{G}^{1/2} \mathbf{C} \xi$

$$\ddot{\xi} + \mathbf{D}\dot{\xi} + \Omega\xi = \mathbf{C}^T \mathbf{G}^{1/2} \mathbf{\Omega}_{\mathbf{c}}^{1/2} \mathbf{\Psi}$$
 (9)

$$\ddot{\mathbf{\psi}} + \mathbf{D_c}\dot{\mathbf{\psi}} + \mathbf{\Omega_c}\mathbf{\psi} = \mathbf{\Omega_c}^{1/2}\mathbf{G}^{1/2}\mathbf{C}\boldsymbol{\xi} \tag{10}$$

By defining
$$\mathbf{E}^{1/2} = \mathbf{G}^{1/2}\mathbf{C}$$
, the MIMO PPF control system can be written as:
$$\begin{bmatrix} \ddot{\xi} \\ \ddot{\psi} \end{bmatrix} + \begin{bmatrix} \mathbf{D} & \mathbf{0} \\ \mathbf{0} & \mathbf{D}_{\mathbf{c}} \end{bmatrix} \begin{bmatrix} \dot{\xi} \\ \dot{\psi} \end{bmatrix} + \begin{bmatrix} \mathbf{\Omega} & -\mathbf{E}^{T/2}\mathbf{\Omega}_{\mathbf{c}}^{T/2} \\ -\mathbf{\Omega}_{\mathbf{c}}^{1/2}\mathbf{E}^{1/2} & \mathbf{\Omega}_{\mathbf{c}} \end{bmatrix} \begin{bmatrix} \boldsymbol{\xi} \\ \boldsymbol{\psi} \end{bmatrix} = \mathbf{0}$$
(11)

Let the Lyapunov Function V be

$$V = \frac{1}{2} \left[\dot{\boldsymbol{\xi}}^T \dot{\boldsymbol{\xi}} + \dot{\boldsymbol{\psi}}^T \dot{\boldsymbol{\psi}} \right] + \frac{1}{2} \left[\boldsymbol{\xi}^T \boldsymbol{\Omega} \boldsymbol{\xi} + \boldsymbol{\psi}^T \boldsymbol{\Omega}_{\mathbf{c}} \boldsymbol{\psi} \right] - \boldsymbol{\xi}^T \mathbf{E}^{T/2} \boldsymbol{\Omega}_{\mathbf{c}}^{T/2} \boldsymbol{\psi}$$
(12)

(12) can be simplified as:

$$V \ge \frac{1}{2} \left[\dot{\xi}^T \dot{\xi} + \dot{\psi}^T \dot{\psi} \right] + \frac{1}{2} \xi^T (\Omega - \mathbf{E}) \xi$$
 (13)

It can be easily proven that if $\Omega - \mathbf{E} > \mathbf{0}$, then V > 0 for all nontrivial $\xi, \psi, \dot{\xi}$, and $\dot{\psi}$. Taking the time derivative of (12) and using (11) yield:

$$\dot{V} = -\dot{\xi}^T \mathbf{D}\dot{\xi} - \dot{\mathbf{\psi}}^T \mathbf{D_c} \dot{\mathbf{\psi}} < 0 \tag{14}$$

It shows in (14) that \dot{V} always below zero. Based on the Lyapunov Theorem, the MIMO PPF control system (11) is Lyapunov Asymptotically Stable iff [16]:

$$\mathbf{\Omega} - \mathbf{E} = \mathbf{\Omega} - \mathbf{C}^T \mathbf{G} \mathbf{C} > \mathbf{0} \tag{15}$$

Knowing Ω and C, (15) can be used to guide the selection of gain G for the MIMO PPF controller.

3.3 Controller performance verification

While the controller gain **G** can be chosen following (15) and ζ_{ck} (k=1,2,3) can be chosen between (0, 1) in principle, better selection of these parameters is crucial for an improved closed-loop damping performance of the system. H_{∞} optimization technique is then used to optimize the selection of the controller parameters via minimizing the vibration influence caused by the disturbance. Define $H_{ij-Cl}(s)$ (i, j=1,2,3) as the closed-loop FRFs of the system. Using generic algorithm, the controller parameters g_k and ζ_{ck} (k=1,2,3) can be optimally selected by obtaining:

$$\min \|H_{ij-Cl}(s)\| \tag{16}$$

The design of the controller parameter matrices, D_c , Ω_c , and G is then finalized.

The resulting MIMO PPF controller performance is verified using Matlab Simulink[®]. In Fig. 6, the red curves show the 3×3 open-loop FRFs, $\overline{H}_{ij}(s)$, and the blue curves show the 3×3 closed-loop FRFs, $H_{ij-Cl}(s)$, utilising the optimized controller parameters. It can be seen from Fig. 6 that, for each mode of concern, the controller provides a sufficient damping to the system that can suppress the vibrations evidently, especially for the dominant 2^{nd} and 3^{rd} modes.

The effectiveness of the PPF control system is further verified via simulation in Fig. 7 where the system outputs $y_i(t)$ (i = 1, 2, 3) computed using $\overline{H}_{ij}(s)$ for the open-loop case are shown in yellow and computed using $H_{ij-Cl}(s)$ for the closed-loop case are shown in pink. The system is subjected to the same sweeping sine wave disturbance w(s) before and after control. It can be seen that the control effects on the three supporting feet of the plate are similar – they all achieve a good vibration suppression with a maximum of 89.826% (19.850 dB) attenuation. Detailed data is given in Table I.

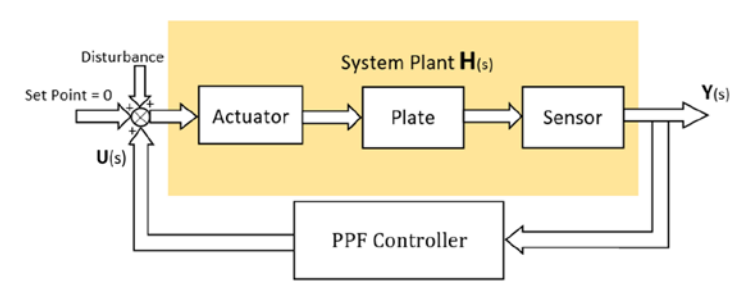


Fig. 5. Block diagram of closed-loop system

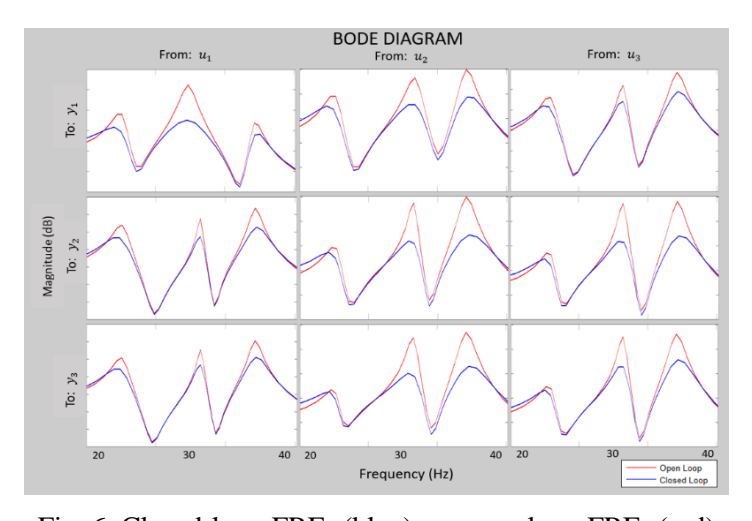


Fig. 6. Closed-loop FRFs (blue) vs. open-loop FRFs (red)

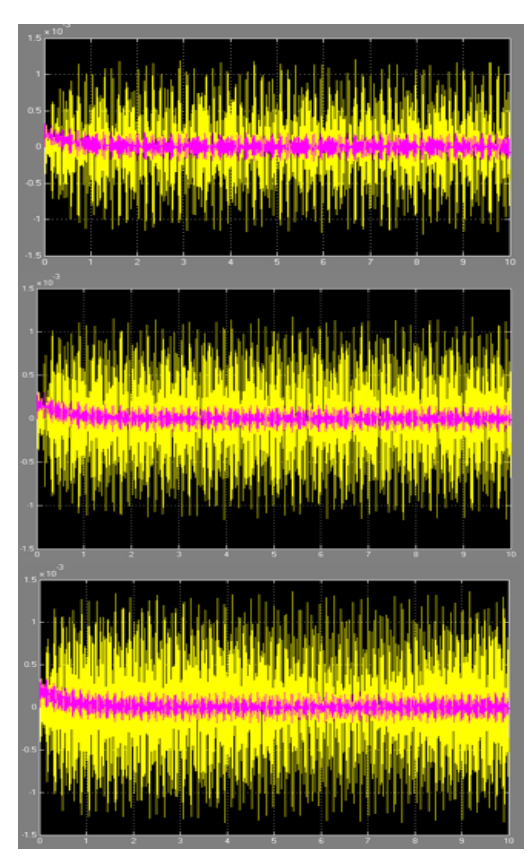


Fig. 7. Simulated system response before (yellow) and after (pink) control

4. **Experimental Result**

The MIMO PPF control scheme is implemented on the physical system of Fig. 1. The controller is realized using dSPACE DS1103, and the input/output signals are measured using NI DAQ that is connected to the disturbance w(s) and the three outputs $y_i(t)$ (i = 1, 2, 3) from T1, T2, and T3 via accelerometers, simultaneously, as shown in Fig. 2. FRFs between the input w(s) and each of the outputs $y_i(t)$ (i = 1, 2, 3) are generated as:

$$T_i(s) = \frac{Y_i(s)}{w(s)}$$
 (i = 1, 2, 3) (17)

 $T_i(s) = \frac{Y_i(s)}{w(s)} \quad (i = 1, 2, 3)$ and are plotted to evaluated the performance of the control system. For open-loop studies, points A and A' in Fig. 2 are opened.

Fig. 8 shows the measured open-loop FRFs in black and the measured closed-loop FRFs in red when the system is subjected to the same disturbance signal. It can be seen that with the MIMO PPF control, the system achieves average attenuations of 16.928 dB (or 85.757%) for the 1st Mode (at 23.6 Hz), 12.345 dB (or 75.859%) for the 2nd Mode (at 28.9 ~ 29.4 Hz), and 10.595 dB (or 70.471%) for the 3rd Mode (at 35.2 Hz). Table II presents the amplitudes of each of the measured outputs before and after control, as well as its corresponding dB attenuation. This set of data is agreeable with that predicted in Fig. 7 (see Table I) for the simulation study of the same situation. The proposed MIMO PPF control of the plate structure in providing sufficient damping to the system's unwanted vibrations and achieving a satisfactory level of vibration isolation is thus evidently demonstrated.

TABLE I. SIMULATED SYSTEM RE-SPONSE IN AMPLITUDE ($\times 10^{-4}$)

Mode 1	T1	T2	Т3
Uncompensated	3.255	2.836	2.236
Compensated	0.588	0.510	0.401
dB attenuation	14.871	14.903	14.922
Mode 2	T1	T2	Т3
Uncompensated	4.261	2.787	2.643
Compensated	0.948	0.531	0.501
dB attenuation	13.057	14.406	14.445
Mode 3	T1	T2	Т3
Uncompensated	4.600	8.110	6.955
Compensated	0.468	0.830	0.715
dB attenuation	19.850	19.799	19.760

TABLE II. EXPERIMENTAL SYSTEM RESPONSE IN dB

Mode 1	T1	T2	Т3
Uncompensated	-62.441	-64.495	-66.375
Compensated	-82.737	-80.235	-81.124
dB attenuation	20.296	15.740	14.749
Mode 2	T1	T2	Т3
Uncompensated	-53.400	-65.384	-62.769
Compensated	-67.995	-78.724	-71.870
dB attenuation	14.595	13.340	9.101
Mode 3	T1	T2	Т3
Uncompensated	-53.859	-48.855	-50.368
Compensated	-64.436	-59.270	-61.160
dB attenuation	10.577	10.415	10.792

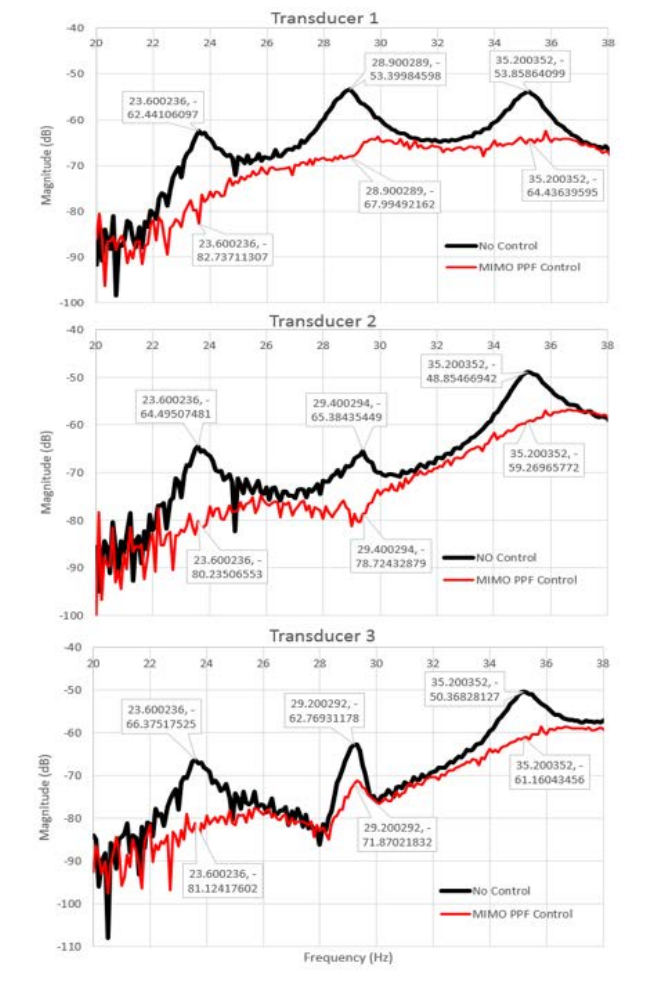


Fig. 8. Experimental system response before (black) and after (red) control

5. Conclusion

In this paper, a MIMO multiple-mode active vibration-cancellation scheme based on PPF control technique for vibration isolation systems is proposed. The MIMO controller is optimized using H_{∞} with generic algorithm, and is successfully applied to the control of the first three modes of a flexible plate bonded with three feet forming a non-ideal asymmetrical structure. The effectiveness of the resulting control system is tested in both simulation and experiment. The proposed method can be extended to larger structures that are potentially vulnerable to environmental disturbances, and the resultant vibration isolation systems are effective in a wider range of frequencies of concern.

REFERENCES

- 1 M. J. Balas. Active control of flexible systems. *Journal of Optinization Theory and Applications*, 25(3): 415-436, 1978.
- 2 I. Friswell and D. J. Inman. The relationship between positive position feedback and output feedback controllers, *Smart Materials and Structures*, 8, 285-291, 1999.
- 3 C. J. Goh and T. K. Caughey. On the stability problem caused by finite actuator dynamics in the collocated control of large space structures. *International Journal of Control*, 41(3): 787-802, 1985.
- 4 L. Meirovitch and H. Baruh. Implementation of modal filters for control of structures. *Journal of Sound and Vibration*, 8, 707-716, 1985.
- 5 H. R. Pota, S. R. Moheimani and M. Smith. Resonant controllers for smart structures, *Smart Materials and Structures*, 11, 1-8, 1999.
- 6 S. R. Moheimani, B. J. G. Vautier and B. Bhilkkaji. Experimental implementation of extended multivariable PPF control on an active structure. *IEEE Transactions on Control Systems Technology*, 14(3), 443-455, 2006.
- 7 A. Zippo, G. Ferrari, M. Amabili, M. Barbieri and F. Pellicano. Active vibration control of a composite sandwich plate, *Composite Structures*, 128,100-114, 2015.
- 8 M. K. Kwak and S. Heo. Active vibration control of smart grid structure by multiinput and multioutput positive position feedback controller. *Journal of Sound and Vibration*, 304, 230-245, 2007.
- 9 G. Ferrari and M. Amabili. Active vibration control of a sandwich plate by non-collocated positive position feedback. *Journal of Sound and Vibration*, 342, 44-56, 2015.
- 10 F. Resta, F. Ripamonti, G. Cazzulani and M. Ferrari. Independent modal control for nonlinear flexible structures: an experimental test rig. *Journal of Sound and Vibration*, 329, 961-972, 2010.
- 11 D. J. Inman. Active modal control for smart structures. Phil. Trans. R. Soc. A 359, 205-219, 2001.
- 12 H. Tjahyadi, F. He and K. Sammut, Multi-mode vibration control of flexible cantilever beam using adaptive resonant control. *Smart Materials and Structures*, 15, 270-278, 2006.
- 13 H. Tjahyadi, F. He, and K. Sammut, M⁴ARC: multi-model-multi-mode adaptive resonant control for dynamically loaded flexible beam structures. *Smart Materials and Structures*, 17(4), 2008.
- 14 J. L. Fanson. An experimental investigation of vibration suppression in large space structures using positive position feedback.
- 15 G. Song, S. P. Schmidt and B. N. Agrawal. Experimental robustness study of positive position feedback control for active vibration suppression. *Journal of Guidance, Control, and Dynamics*, 25(1), 179a-182, 2002.
- 16 S. Skogestad and I. Postlethwaite. Multivariable feedback control: analysis and design, 2, New York: Wiley, 2007.